Downward water mobility in applied smoldering

Jiahao Wang[a*], Marco A. B. Zanoni[a], Tarek L. Rashwan[b, c], José L. Torero[c], Jason I. Gerhard[a, ǂ]

[a]*Department of Civil and Environmental Engineering, The University of Western Ontario, London, Ontario, N6A 5B9, Canada*
[b]*School of Engineering & Innovation, The Open University, Milton Keynes, MK7 6AA, UK*
[c]*Department of Civil, Environmental and Geomatic Engineering, University College London, London, WC1E 6BT, UK*

Abstract

Applied forward smoldering is used in energy-efficient combustion systems to treat high moisture content waste. However, these systems must be operated in a robust manner far from quenching conditions. Quenching can lead to process failure; therefore, it is critical to accurately resolve water transport in different phases throughout space and time to optimize these smoldering systems. In this work, liquid mobility was integrated into a validated smoldering model that previously only included immobile water. The model was applied to a vertical reactor with an upward propagating forward smoldering reaction. Comparisons between mobility and non-mobility models indicate that the water mobility must be considered to accurately simulate both smoldering ignition and propagation in systems with high water saturations. Water mobility during smoldering can lead to two opposing effects: i) water accumulation at the bottom of the pack, which results in large ignition times or ignition failure; and ii) downward displacement of re-condensed water ahead of the smoldering front, which results in robust propagation with high peak temperatures and front velocities. Finally, a sensitivity analysis revealed the influence of operational parameters on water mobility, which can control the fate of smoldering. Tall fuel pack, high permeability, well-sorted particles, and low capillary-bound saturation were found to significantly accelerate water downward mobility and inhibit ignition. Nevertheless, extending the duration of the initial convective heating process and reducing the packing height favored ignition. These results are highly relevant to current industry applications and address a key knowledge gap in smoldering research.

Keywords: Liquid mobility; Smoldering; Energy balance; Ignition; Extinction

*Corresponding author.

ǂ Deceased

Information for Colloquium Chairs and Cochairs, Editors, and Reviewers

1) Novelty and Significance Statement

Smoldering is proven to be an effective approach towards waste to energy. Key to the successful use of smoldering as a waste destruction technique is the stability of the reaction front. Excess water in high moisture content wastes is a major energy sink that can lead to reaction quenching and process failure. Therefore, water dynamics need to be well-understood to design efficient smoldering systems. The thermal effects of water on smoldering have been studied previously; nevertheless, the fate of smoldering has been demonstrated to be directly related to processes that evolve in space and time – which are poorly understood. Quenching is very sensitive to heat and mass transfer occurring in the porous media far from the reaction. Thus, water mobility is key. This paper is the first effort to address water mobility in the context of smoldering combustion. The conclusions presented here are widely applicable to all smoldering processes including other liquid compounds, e.g., crude oil sludge waste.

2) Author Contributions

- J. Wang: conceptualization, funding acquisition, methodology, formal analysis, writing – original draft.
- M. A. B. Zanoni: conceptualization, supervision, methodology, writing – review & editing.
- T. L. Rashwan: funding acquisition, supervision, methodology, writing – review & editing.
- J. L. Torero: supervision, methodology, writing – review & editing.
- J. I. Gerhard: funding acquisition, resources.

3) Authors' Preference and Justification for Mode of Presentation at the Symposium

The authors prefer **OPP** presentation at the Symposium for the following reasons:

- Focusing on managing wet wastes, where waste to energy is well-aligned with the theme of energy transition.
- Highlighting the impact of water mobility on smoldering is best presented through visual animations in an oral format.
- The impact of spatial heat exchange on smoldering is poorly understood; thus, is a subject of strong academic discussion.

Nomenclature

Latin Letters

$A_{s,sp}$	Surface area of sphere, m^2
A_{cs}	Cross-section area, m^2
D_g	Gas diffusion coefficient, m^2 s^{-1}
$\dot{E}$	Energy rate, J s^{-1}
h_{sg}	Interfacial heat transfer coefficient, W m^{-2} K^{-1}
k	Thermal conductivity, W m^{-1} K^{-1}
k_p	Intrinsic permeability, m^2
$k_{p,r}$	relative permeability, m^2
$\dot{m}_w'''$	Evaporation rate, kg m^{-3} s^{-1}
P	Pressure, Pa
P_c	Capillary pressure, Pa
R_{GAC}	Reaction rate, s^{-1}
S_b	Capillary-bound saturation, -
S_r	Residual saturation, -
S_w	Water saturation, -
T	Temperature, K
u	Velocity, m s^{-1}
U	Global heat loss coefficient, W m^{-2} K^{-1}
ν_{O2}	Stoichiometric coefficient, kg.O$_2$ kg.fuel^{-1}

Greek Symbols

ρ	Density, kg m^{-3}
ϕ	Porosity, -
μ	Dynamic viscosity, Pa.s
δ, γ	Empirical constant, -
λ	Pore size distribution index, -

Subscripts/Superscript

Cl	Cylinder
0	Ambient/Initial
w,v,g	Water, vapor, gas

1. Introduction

Smoldering is a flameless form of combustion driven by the oxidation of a condensed phase fuel [1]. Accidental smoldering fires can cause catastrophic losses (e.g., wildfires), while applied smoldering is emerging for soil remediation and waste management purposes. To date, numerous laboratory and pilot tests have demonstrated that high moisture content wastes (HMWs) can be treated via smoldering in a cost-effective manner, such as sewage sludge [2-4], feces [5] and food wastes [6]. Most of these wastes contain moisture content above 50 wt% and exhibit low heating values (~20 kJ/g), posing a challenge to conventional thermal methods and energy recovery.

Applied smoldering of HMWs is designed to operate as a "self-sustained" process, which requires two distinct stages [7]. The first stage is pre-heating, where heat is provided to a small, localized area (referred to as the ignition zone). The external heater causes a rise in local temperature until the wet wastes dry and then reach the ignition point [8]. The second stage introduces airflow to ignite smoldering. During this phase, the smoldering front propagates in a self-sustained manner without additional external energy input, provided the local energy generation rate overwhelms local heat losses. Local heat losses result from the energy balance in and out of the reaction zone from other areas of the system. Thus, mobility of any liquid compound (e.g., water) affects heat losses.

The self-sustained nature of smoldering makes it an energy-efficient technology for processing HMWs. However, in both stages, it is crucial that the energy provided by the heater or generated from the oxidation process is sufficient to evaporate water and sustain smoldering, i.e., achieve a positive energy balance [9]. Under this condition, a dry zone appears ahead of the smoldering propagation (i.e., buffer zone) so the combustion reaction only encounters dry fuel [8].

Nevertheless, the water saturation (S_w) distribution is non-uniform in smoldering systems, which evolves over time and space within the heated porous medium due to phase change [5, 8, 10] and gravitational drainage [11]. The former aspect has been thoroughly studied. Yermán et al. [5] and Wang et al. [8] showed that water re-condensation can increase the local S_w ahead of smoldering significantly beyond the initial condition (e.g., up to 5×) and cause extinction. This water accumulation can slow down drying processes, and thereby suppress the dry buffer between smoldering and wet regions. A minimum dry buffer thickness is required to achieve stable smoldering [8].

In addition, water can move downwards due to gravity and accumulate near the ignition zone [2]. The unintended water accumulation might require a prolonged heating time for complete local evaporation, which would require additional energy supply and reduce economic efficiency. However, water mobility in porous media is challenging to predict, where air and water form an interlinked two-phase flow governed by highly non-linear equations [12]. The mobility of each phase relies on the interdependence of capillary pressures and relative permeabilities in the pore space, which is a function of system properties like initial water saturation ($S_{w,0}$), intrinsic permeability (k_p), packing height (H), and capillary-bound saturation (S_b). Note that S_b defines the threshold where capillary forces resist mobility, and water cannot be displaced without a phase change. Therefore, mobility can be neglected when $S_w < S_b$ [12]. While the effect of two-phase flow on smoldering systems has been observed experimentally [2-6], it is not yet well-understood. Thus, a modelling approach is necessary to comprehensively understand the impact of water mobility on smoldering systems, which can ultimately govern treatment success.

This study aims to extend the utility of a previously validated one-dimensional wet smoldering model from Wang et al. [8] by adding water mobility physics. A series of experiments were performed to explore water mobility and validate model results. A sensitivity analysis was also conducted to investigate the role of key system parameters on water dynamics and smoldering performance. Altogether, this updated model provides novel insights that are critical in optimizing HMW smoldering systems.

Table 1
Summary of all model and experimental cases.

Case (-)	Simulated water mobility?	$S_{w,0}$ (%)	C_f [a] (%)	$u_{g,in}$ (cm/s)	H (cm)	S_b (%)	λ	k_p ($x10^{-10}$ m^2)	t_g, t_h (s)	SS? [b]
1	-	20	3	5	73	14	2.5	5	6000, 6480	SS
2	-	30	3	5	73	14	2.5	5	6120, 6720	SS
3	✓ Validation	20	3	5	73	14	2.5	5	6000, 6480	SS
4	✓ Validation	30	3	5	73	14	2.5	5	6120, 6720	SS
5	✓	30	3	5	36.5	14	2.5	5	6120, 6720	SS
6	✓	30	3	5	80	14	2.5	5	6120, 6720	SS
7	✓	30	3	5	73	7	2.5	5	6120, 6720	NSS [c]
8	✓	30	3	5	73	28	2.5	5	6120, 6720	SS
9	✓	30	3	5	73	14	1.25	5	6120, 6720	SS
10	✓	30	3	5	73	14	5	5	6120, 6720	SS
11	✓	30	3	5	73	14	2.5	2.5	6120, 6720	SS
12	✓	30	3	5	73	14	2.5	10	6120, 6720	SS
13	✓	30	3	5	73	7	2.5	5	7400, 8000	NSS
14	✓	30	3	5	73	7	2.5	5	6120, 8000	SS
15	✓	30	3	5	36.5	7	2.5	5	6120, 6720	SS

[a] Fuel concentration [kg.O_2 kg.fuel^{-1}]; [b] Self-sustained?; [c] Non-self-sustained.

2. Methodology

The experimental setup in Fig. 1 used water, sand, and granular activated carbon (GAC). Material properties and established experimental procedures are detailed in [7-8]. A radiative heater was used for ignition. When the ignition point was reached, air was injected at t_g to support upward smoldering. Once self-sustaining smoldering was established, the heater was turned off at t_h . The experiments included continuous measurements of axial temperatures via 25 thermocouples (TCs) at 3 cm intervals, which were used for the model validation [8]. Refer to Supplementary Material (SM) Section S1 for more details about the experimental setup.

Two wet smoldering conditions were simulated in COMSOL (see Table 1). Cases #1-2 simulated wet smoldering without mobility. Cases #3-4 considered water mobility and were then validated against experiments. Case #4 served as the base case for the numerical sensitivity analysis, where Cases #5-15 were conducted to study the impacts of packing height (*H*), capillary-bound saturation (S_b), pore size distribution index (λ), and permeability (k_p). The model based on Wang et al. [8] addressed GAC smoldering coupled with water phase change processes, while the water mobility addition followed key methodologies from Gerhard and Kueper [12].

2.1 Governing equations

Eqs. 1-7 in Table 2 represent the conservation equations for the solid, water, and gas phases. All symbols are defined in the Nomenclature. The governing equations are briefly discussed here, and

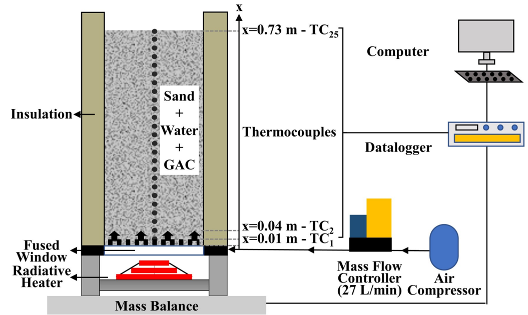

Fig. 1: Schematic of the experimental setup.

further details on the model input parameters and boundary conditions can be found in SM Sections S2-4 and [8]. Eqs. 1-4 account for the conservation of mass for GAC, water, vapor, oxygen, and total gas mixture. GAC is a by-product of coal pyrolysis, and its smoldering reaction can be modelled with a 1-step oxidation reaction in Eq. 8 [13]. The water velocity, u_w, was governed by gravity and capillary pressure, while water evaporation was simulated by the water evaporation rate ($\dot{m}_w'''$). Eqs. 6-7 solved local thermal non-equilibrium energy transport between solid and gas phases; however, the solid and liquid phases were assumed to be in local thermal equilibrium. This assumption is reasonable since water flowed slowly compared to gas ($u_w << u_g$) [8, 12]. In this work, when the local S_w was beyond 60%, γ was set to 0.2 in the entire domain to consider the effects of fast water phase change; otherwise, γ followed Eq. 10. More details on this methodology can be found in [8].

2.2 Two-phase flow

Table 2
Governing equations.

Equations	No.
$\frac{\partial(Y_{GAC})}{\partial t} = -R_{GAC}$	Eq. 1
$\phi\rho_w \frac{\partial(S_w)}{\partial t} = -\rho_w \frac{\partial(u_w)}{\partial x} - \dot{m}_w'''$	Eq. 2
$\phi \frac{\partial(S_g\rho_g Y_v)}{\partial t} + \frac{\partial(\rho_g u_g Y_v)}{\partial x} = \phi \frac{\partial}{\partial x}\left(S_g\rho_g D_{g,wv}\frac{\partial Y_v}{\partial x}\right) + \dot{m}_w'''$	Eq. 3
$\phi \frac{\partial(\rho_g S_g Y_a Y_{O_2})}{\partial t} + \frac{\partial(\rho_g u_g Y_a Y_{O_2})}{\partial x} = \phi \frac{\partial}{\partial x}\left(\rho_g S_g Y_a D_{g,O_2}\frac{\partial Y_{O_2}}{\partial x}\right) - \rho_{GAC,b} v_{O_2} R_{GAC}$	Eq. 4
$\phi \frac{\partial(S_g\rho_g)}{\partial t} + \frac{\partial(\rho_g u_g)}{\partial x} = \rho_{GAC,b}R_{GAC} + \dot{m}_w'''$	Eq. 5
$(\rho C_p)_{eff}\frac{\partial T_s}{\partial t} + \rho_w C_{pw} u_w \frac{\partial T_s}{\partial x} = \frac{\partial}{\partial x}\left(k_{eff}\frac{\partial T_s}{\partial x}\right) - U\left(\frac{A_{s,cl}}{V_{cl}}\right)(T_s - T_0) + h_{sg}\left(\frac{A_{s,sp}}{V_{sp}}\right)(T_g - T_s) - \rho_{GAC,b}\Delta H_{GAC}R_{GAC} - \Delta H_{evap}\dot{m}_w'''$	Eq. 6
$\phi S_g\left(\rho_g C_{p_g}\right)\frac{\partial T_g}{\partial t} + \rho_g C_{p_g} u_g \frac{\partial T_g}{\partial x} = \phi S_g \frac{\partial}{\partial x}\left(k_g\frac{\partial T_g}{\partial x}\right) + h_{sg}\left(\frac{A_{s,sp}}{V_{sp}}\right)(T_s - T_g) + \dot{m}_w''' C_{p_v}(T_s - T_g)$	Eq. 7
$GAC + v_{O_2}O_2 \xrightarrow{R_{GAC}} Gas,\ R_{GAC} = A_{GAC}exp\left(-\frac{E_{GAC}}{RT_s}\right)(Y_{GAC})(Y_{O_2})$	Eq. 8
$k_{eff} = \delta\,[(1-\phi)(k_s + k_{rad}) + (\phi S_w)k_w + \phi_{GAC}k_{GAC}],\ t \le t_g, \delta = 6;\ t > t_g, \delta = 1$	Eq. 9
$(\rho C_p)_{eff} = \gamma[(1-\phi)\rho_s C_{ps} + (\phi S_w)\rho_w C_{pw} + (\emptyset_{GAC})\rho_{GAC}C_{pGAC}],\ \gamma = 0.56\,(S_{w,0})^{-0.19}$	Eq. 10
$u_g = -\frac{k_{rg}k_p}{\mu_g}\left(\frac{\partial P_g}{\partial x} - \rho_g g\right)$	Eq. 11
$u_w = -\frac{k_{rw}k_p}{\mu_w}\left(\frac{\partial P_w}{\partial x} - \rho_w g\right), S_w > S_{w,b}$	Eq. 12

In this study, it was assumed that when S_w was lower than the capillary-bound saturation, S_b (14%), water was immobile [12]. Consequently, the two-phase flow mobility feature was only activated when $S_w \geq$ 14%, where u_g and u_w were calculated from Eqs. 11-12. They were coupled through the capillary pressure-saturation relationship $P_C = P_g - P_w$, which followed Brooks-Corey Capillary pressure curve and associated relative permeability in SM Section S3.

2.3 *Global Energy Balance*

A global energy balance was applied:

$$\dot{E}_{net} = \dot{E}_{in} + \dot{E}_{evap} + \dot{E}_{oxid} + \dot{E}_{loss} + \dot{E}_{out} \quad (13)$$

where $\dot{E}_{net}$ represents the global net energy rate stored in the porous media, which is the sum of five energy rates: heater input energy ($\dot{E}_{in}$), energy consumed by evaporation ($\dot{E}_{evap}$), oxidation energy generated ($\dot{E}_{oxid}$), system heat losses ($\dot{E}_{loss}$), and energy out through the effluent gas ($\dot{E}_{out}$). Each term was defined in [8, 14] and detailed in SM Table S3. A positive $\dot{E}_{net}$ is needed for self-sustained smoldering.

3. Results and Discussion

3.1 *Model Validation*

Fig. 2 shows the simulated temperature and S_w computed with and without water mobility compared to the experimental results (i.e., Cases #1-4). Note that the non-mobility model was validated with low saturation experiments in [8]. After air injection, smoldering was initiated and propagated in a self-sustained manner at similar smoldering front velocities with and without mobility. For example, the case of S_w= 30% had average smoldering velocities of 0.619 ± 0.048 cm.min^{-1} (two experimental repeats), 0.662 cm.min^{-1} (mobility model), and 0.600 cm.min^{-1} (non-mobility model); and peak temperatures of 847 ± 44 °C (two experimental repeats), 783 °C (mobility model) and 765 °C (non-mobility model). Moreover, both models captured the ~50 °C plateau, which resulted from the water re-condensation ahead of smoldering [8]. These similar results suggest that the direct impact of water mobility on the "smoldering propagation" stage was relatively small.

Nevertheless, the "pre-heating" stage (i.e., with air off) can only be simulated with the mobility model. The water in the bottom of the pack started to boil at 100 °C due to radiative heating. Then the produced vapor moved upwards due to buoyancy, which condensed in the upper cold regions, releasing the latent heat and increasing temperatures until boiling [10]. The succession of crossing temperature profiles at 100 °C represents the propagation of the condensation front ahead of water boiling (Fig. 2b). However, in the mobility model, water in the upper region above S_b could move downwards and accumulate at the bottom of the pack, as shown by a

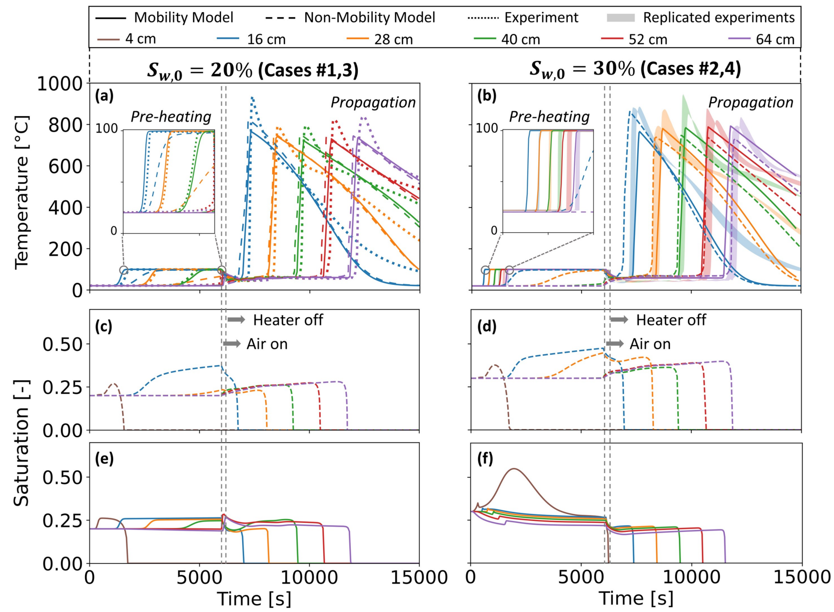

Fig. 2: Comparisons between the mobility model (solid lines), non-mobility model (dashed lines), and experiments (dotted lines, and shadings showing the ranges for two experimental repeats) for Cases #1-4. (a-b) Temperature and (c-f) water evolutions versus time. Colors describe the measurement positions of temperatures and water saturations at 0.12 m intervals.

significant increase in S_w at x = 4 cm (e.g., 60% vs. 30% in Fig. 2f and 2d, respectively). This accumulation produced more vapor that transported upwards and further enhanced the release of the water latent heat. As a result, water mobility caused the condensation front to propagate faster, and thus the entire column was rapidly heated to 100 °C, compared to the case without mobility (Fig. 2a, b). In addition, the condensation front propagated quicker in Case #4 ($S_{w,0}$=30%) than Case #3 ($S_{w,0}$=20%); again, due to water mobility. Case #4 had a $S_{w,0}$ well-above S_b (30% vs. 14%), i.e., it caused more water accumulation in the bottom and faster vapor production than Case #3. Besides, the maximum S_w at x = 4 cm was doubled in the mobility model than the non-mobility model for $S_{w,0}$=30%, while the case of $S_{w,0}$=20% had a similar bottom S_w in both models. These results demonstrate that water mobility is important at high saturations and must be simulated at these conditions to predict key smoldering dynamics.

Although the water boiling rate increased due to water mobility, the time to dry the bottom lengthened with mobility. The drying time at x = 4 cm for the $S_{w,0}$ =30% condition was predicted to be 6000 s (mobility, Case #4) and 1700 s (non-mobility, Case #2). This increased drying time aligns well with common experimental trends observed in HMWs smoldering [2-6], revealing the water migration rate is much faster than the increased boiling rate. Moreover, this water accumulation can create challenging ignition conditions. For instance, it took a longer time for x = 16 cm (the blue TC in Fig. 2b) to ignite after considering mobility, suggesting weaker ignition.

In contrast, the downward water migration decreased S_w across space away from the bottom (x > 4 cm in Fig. 2d, f), which favored smoldering during the propagation stage. A higher peak temperature and faster smoldering front velocity were observed in the mobility model than the non-mobility model (783 vs. 765 °C and 0.662 vs. 0.600 cm.min^{-1}, respectively, Fig. 2b). This finding suggests that the major obstacle in smoldering HMWs might be the long drying period during pre-heating. Once it is overcome, smoldering propagation is successful as less S_w remains in the system due to initial mobility.

3.2 Water and vapor movement

Fig. 3 illustrates the migration of water and vapor during the wet smoldering process for the base case (#4). At t = 0 s, the entire domain is at $S_{w,0}$ (30%) and there was no water vapor in the gas phase. Then, water migrated downwards where local S_w > S_b (14%). This resulted in a non-uniform water distribution, reducing S_w at the top while increasing S_w at the bottom (e.g., 75% in Fig. 3d). With the heater turned on, accumulated water in the bottom started to boil and produce vapor, leading to a fully saturated vapor (i.e., Y_v = 100%). Due to the vapor pressure gradient, vapor moved upwards and condensed in the upper cold region away from the heater. At the condensation front, Y_v immediately reduced from 100% to 0% while the local S_w increased, corresponding to a small peak in the S_w profile (Fig. 3d) and the temperature rose to 100 ℃ (Fig. 3e). At t = 2000 s, the condensation front reached the top of the pack, and

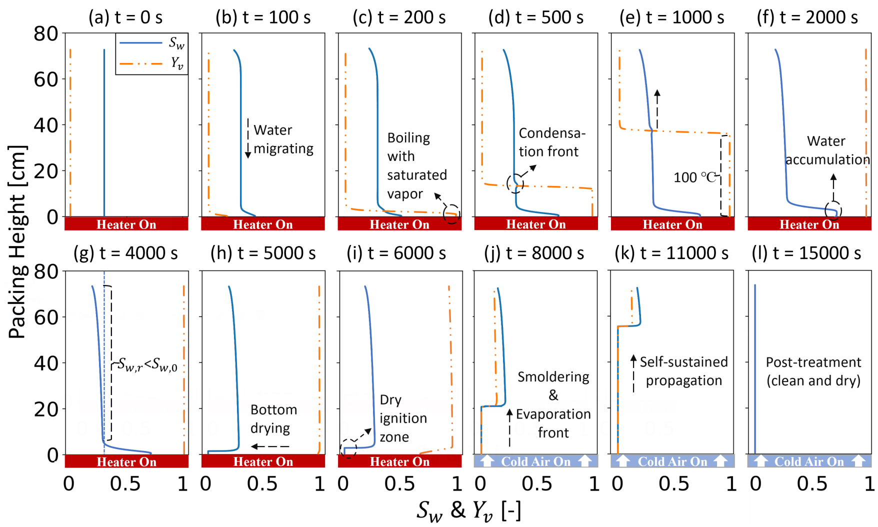

Fig. 3: The predicted water and vapor saturation distribution for base case (#4) considering water mobility. The blue solid lines and orange dotted-dashed lines represent the local water saturation (S_w) and vapor saturation (Y_v), respectively. The dotted blue line is $S_{w,0}$.

the entire pack was boiling at 100 °C, with vapor leaving the top outlet. However, the water velocity was faster than the evaporation rate, which led to water accumulation in the bottom (as discussed above in Section 3.1 and shown in Fig. 2f).

At t = 4000-5000 s, the water accumulation height decreased as the water mobility became slower than the evaporation. By this time, a large amount of water was evaporated out, and the system exhibited a relatively low residual saturation relative to the initial ($S_r < S_{w,0}$, Fig. 3g). S_r represents the maximum S_w that the porous material can retain against gravity drainage, which is greater than S_b (see SM Section S6). Below S_r, water can cling to the solid due to capillary forces, and therefore water is immobile [15]. This finding is novel for both research and applications, as it quantifies how $S_{w,0}$ might not limit smoldering propagation because water mobility enhances the evaporation and decreases overall S_w to S_r before the ignition.

After 6000 s of heating, a 4 cm dry ignition zone appeared, and smoldering ignition was achieved when airflow was injected (Fig. 3i). The water evaporation front was driven by the smoldering front, accelerating the drying process in the entire system. At t = 15000 s, the reaction front reached the top of the pack, leaving behind dry and fuel-free porous media.

3.3 Sensitivity Analysis

Previous studies have identified packing height (H), capillary-bound saturation (S_b), pore size distribution index (λ), and intrinsic permeability (k_p) as key factors influencing water mobility within porous media [12, 16]. These parameters are not only crucial to understanding water dynamics but also allow engineers to fine-tune wet smoldering systems. Consequently, these properties, using practical values [1-10, 12, 13-14, 16], were chosen for a sensitivity analysis of water mobility across eight cases. Each parameter was varied by half or double the base case value (#4), except the packing height, where a high H condition was only increased from 73 to 80 cm to optimize computational time (Fig. 4).

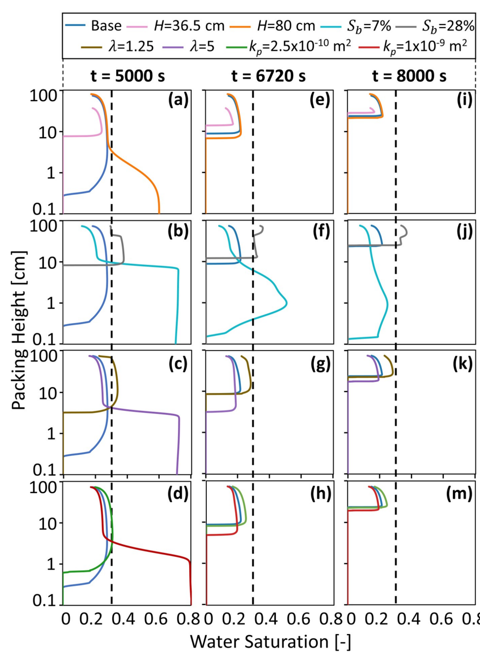

Fig. 4: Spatial water distribution for the sensitivity analyses at 5000, 6720, and 8000 s. The vertical dashed black line indicates $S_{w,0}$.

Fig. 4a-d show S_w distributions at t = 5000 s (air off). At this time, the bottom of the pack in the base case (#4) was dried with a 0.2 cm dry zone. However, a small increase of H to 80 cm led to a substantial rise in the bottom S_w (60%). The extra water height effectively increased the water migration rate, and more water flowed downwards and accumulated in the bottom (Fig. 4a). In contrast, a decrease in H to 36.5 cm reduced water migration, and a 10 cm dry zone was observed after the same pre-heating time. This finding agrees with [16], revealing the importance of packing height in HMW smoldering.

As shown in Fig. 4b-c, low S_b and high λ cases also accelerated the downward water mobility, which accumulated water in 7 and 3 cm thick pools, respectively, with S_w = 70% (note, $S_{w,0}$ = 30%). A porous medium with a low S_b means that the pores hardly retain water; thus, water can easily move downwards with gravity. A high λ represents a porous medium that is composed of well-sorted particles with a homogeneous pore size, i.e., without tiny pores inhibiting water flow. Therefore, water moved through the well-sorted pores more freely. Nevertheless, even though water pooled at different heights, neither S_b nor λ affected the S_w of the water pool, which was fixed at 70%. This constant pool S_w emerged because water can only invade pores and increase S_w when the water pressure exceeds the displacement pressure, which is limited by the porosity, permeability, and surface tension between water and air [12]. Therefore, as expected, Fig. 4d shows that an increase in the S_w of water pool (80% vs. 70%) resulted from increasing the permeability. Moreover, increased downward water mobility drained water from the upper region, as evidenced by a lower S_w in high H, λ, k_p, and low S_b conditions above x = 10 cm (Fig. 4a-d).

At t = 6720 s, the heater was turned off (airflow was turned on at 6120 s) and smoldering propagated in a self-sustained condition, where $\dot{E}_{net}$ was positive (Eq. 13). That is, the energy rate generated by oxidation exceeded the energy consumption rate by water evaporation and system heat losses. Here, the magnitude of $\dot{E}_{net}$ represents the robustness of smoldering ignition. In Fig. 5, base case (#4) had a $\dot{E}_{net}$ around 640 J/s. However, the enhanced downward water mobility decreased $\dot{E}_{net}$ and weakened ignition. For example, in the case of S_b = 7%, the bottom ignition zone was not completely dried (Fig. 4f) and thus smoldering ignition was not successful, with a $\dot{E}_{net}$ of -270 J/s. On the other hand, stronger ignition occurred with higher $\dot{E}_{net}$ when the water mobility and accumulation were reduced (e.g., with low H and high λ).

Fig. 5 also shows $\dot{E}_{net}$ at 8000 s when smoldering reached the end of the pack. This figure shows the impact of mobility on $\dot{E}_{net}$ at this time was diminished in most cases due to the similarities in remaining S_w profiles (see Fig. 4i-m). This remaining S_w was dominated by the water mobility and water re-condensation in the upper cold region [8]. The enhanced water mobility could mitigate water re-condensation and lead to a low remaining S_w and more robust smoldering. For instance, Case #10 with well-sorted particles (λ = 5) had substantial downward water migration, and a large fraction of the water was evaporated during pre-heating. These dynamics led to a much lower remaining S_w than Case #8 with S_b = 28%, i.e., 10% vs. 40%, respectively (Fig. 4j-k). The lower S_w thereby fostered more robust smoldering in Case #10 than #8 (650 J/s vs. 350 J/s, respectively, in Fig. 5). Similar behavior was found for the other cases. The peak temperatures and front velocities of all the cases analyzed are available in SM Table S4.

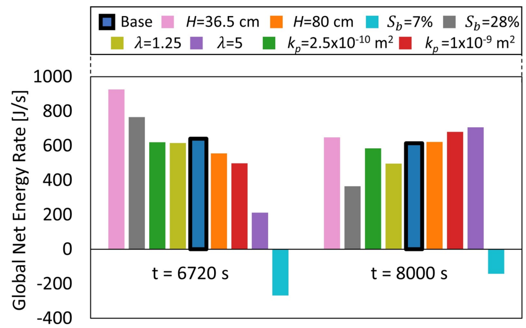

Fig. 5: Global net energy rates from the sensitivity analyses at 6720 s and 8000 s.

Altogether, downward water mobility accumulates more water initially in the base that must be evaporated during pre-heating by an external heater, which lowers the remaining S_w to hinder subsequent smoldering. Therefore, if ignition is successful, initial downward water mobility can promote smoldering propagation and increase system robustness with a high $\dot{E}_{net}$. This is a key finding of this study.

3.4 Re-ignition

Three additional cases were conducted to investigate extinction of Case #7: air-on time (t_g), heater-off time (t_h), and packing height (H).

Case #13 extended both airflow and heating times by ~ 21 minutes (t_g= 7400 s, t_h= 8000 s). Fig. 6b shows that a longer pre-heating time was not sufficient to dry the bottom of the pack; therefore, ignition was unsuccessful. Nevertheless, Case #14 increased t_h (8000 s) but kept t_g (6120 s) fixed – like in the Case #7 – resulting in successful ignition (Fig. 6c). This approach extended the convective heating time (i.e., the period when air and heater were both on), which enhanced water evaporation under the forced airflow. This condition accelerated the drying processes and enabled ignition before the heater was turned off. The comparison between Cases #13 and #14 is important for industrial applications as it suggests that when ignition failures occur due to water quenching, convective heaters should be used for re-ignition. Besides, this observation confirmed the conclusion of Section 3.3, i.e., once ignition is successful, smoldering should be sufficiently robust to propagate through wet fuel regions.

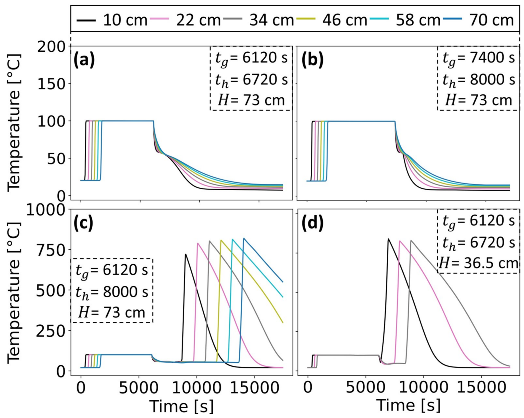

Fig. 6: Different strategies to re-ignite Case #7 (a): (b) increasing pre-heating stage; (c) increasing convective heating stage; and (d) halving the packing height.

Finally, when the packing height was decreased by half (Case #15, Fig. 6d), smoldering ignition was also successful because less water accumulated at the pack bottom. This finding is important in designing smoldering reactors to best treat HMWs.

Conclusion

In this work, water mobility was integrated into a smoldering numerical model with immobile water dynamics. This new model was successfully validated with experimental data. The simulations showed that water mobility must be considered to accurately simulate smoldering ignition and propagation under high water saturations. Water mobility was shown to lead to i) severe water accumulation near the heater, which can inhibit ignition; and ii) reduced water content ahead of the smoldering front, which can favor subsequent smoldering propagation. These observations indicate that water mobility predominantly occurs in the initial phase of ignition and significantly influences ignition success. The fundamental finding should be applicable across a variety of fuels and smoldering systems, particularly in upward configurations.

Furthermore, the model revealed the important role of operating properties on water mobility and thus the fate of smoldering performance. A porous material characterized by high permeability, homogeneity, and low capillary-bound saturation could accelerate water mobility and create challenging ignition conditions. However, extending the convective heating time and decreasing the packing height are two viable strategies to promote smoldering ignition.

Overall, this work provides unique insights into the critical role of water mobility in applied smoldering systems. The observations presented in this work will help researchers and engineers better understand and optimize these systems. Moreover, the conclusions presented here are widely applicable to smoldering in other contexts (e.g., wildfires with wet fuels). However, more complex fuels with different water dynamics, such as bonded water, require further investigation.

Declaration of competing interest

The authors declare that they have no known competing financial interests or personal relationships that could have appeared to influence the work reported in this paper.

Acknowledgements

Funding was provided by the Natural Sciences, the Engineering Research Council of Canada, the Royal Society (RG\R2\232528), and The Open University through Engineering & Innovation Research Funding, Higher Education Innovation Funding Knowledge Transfer Vouchers, and the Open Societal Challenges Programme in support of the SPLICE challenge, and Mitacs Globalink. We appreciate support from Chris Power, Zia Miry, Angelos Almpanis, Joshua Brown, Taryn Fournie, Shuyang Wang, and Huiyi Yang.

Supplementary material

Supplementary material can be found online.

References

[1] J.L. Torero, J.I. Gerhard, M.F. Martins, M.A.B. Zanoni, T.L. Rashwan, J.K. Brown, Processes defining smouldering combustion: integrated review and synthesis, Prog. Energy Combust. Sci. 81 (2020) 100869.

[2] T.L. Rashwan, J.I. Gerhard, G.P. Grant, Application of self-sustaining smouldering combustion for the destruction of wastewater biosolids, Waste Manage. 50 (2016) 201-212.

[3] T.L. Rashwan, T. Fournie, J.L. Torero, G.P. Grant, J.I. Gerhard, Scaling up self-sustained smouldering of sewage sludge for waste-to-energy, Waste Manage. 135 (2021) 298-308.

[4] T.L. Rashwan, T. Fournie, M. Green, A.L. Duchesne, J.K. Brown, G.P. Grant, J.L. Torero, J.I. Gerhard, Applied smouldering for co-waste management: Benefits and trade-offs, Fuel Process. Technol. 240 (2023) 107542.

[5] L. Yermán, R.M. Hadden, J. Carrascal, I. Fabris, D. Cormier, J.L. Torero, J.I. Gerhard, M. Krajcovic, P. Pironi, Y.-L. Cheng, Smouldering combustion as a treatment technology for faeces: exploring the parameter space, Fuel 147 (2015) 108-116.

[6] Z. Song, T. He, M. Li, D. Wu, F. You, Self-sustaining smoldering as a novel disposal approach for food waste with high moisture content, Fuel Process. Tech- nol. 228 (2022) 107144.

[7] J. Wang, G.P. Grant, J.I. Gerhard, The influence of porous media heterogeneity on smouldering remediation, J. Contam. Hydrol. 237 (2021) 103756.

[8] J. Wang, M. A. B. Zanoni, J. L. Torero, J. I. Gerhard, Understanding the role of water evaporation and condensation in applied smoldering systems, Combust. Flame 253 (2023) 112780.

[9] M.A.B. Zanoni, J.L. Torero, J.I. Gerhard, Experimental and numerical investigation of weak, self-sustained conditions in engineered smouldering combustion, Combust. Flame 222 (2020) 27-35.

[10] M.A.B. Zanoni, J. Wang, J.L. Torero, J.I. Gerhard, Multiphase modelling of water evaporation and condensation in an air-heated porous medium, Appl. Therm. Eng. 212 (2022) 118516.

[11] M. G. Letts, N. T. Roulet, N. T. Comer, M. R. Skarupa, D. L. Verseghy, Parametrization of Peatland Hydraulic Properties for the Canadian Land Surface Scheme, ATMOS. OCEAN, 38 (2000).

[12] J. I. Gerhard, B. H. Kueper, Relative permeability characteristics necessary for simulating DNAPL infiltration, redistribution, and immobilization in saturated porous media, Water Resour. Res. 39 (2003).

[13] M.A.B. Zanoni, J. Wang, J.I. Gerhard, Understanding pressure changes in smouldering thermal porous media reactors, J. Chem. Eng. 412 (2021) 128642.

[14] M.A.B. Zanoni, J.L. Torero, J.I. Gerhard, Determining the conditions that lead to self-sustained smouldering combustion by means of numerical modelling, Proc. Combust. Inst. 37 (2019) 4043-4051.

[15] A. I. Johnson, Specific yield-compilation of specific yields for various materials, Geological survey water supply paper 1662-D, (1967)

[16] L. Kinsman, J.L. Torero, J.I. Gerhard, Organic Liquid Mobility induced by smoldering remediation, J. Hazard. Mater. 325 (2017) 101-112.